Molecular Simulation, Vol. 32, No. 15, 30 December 2006, 1207–1212

Taylor & Francis
Taylor & Francis Group

XPS and *ab initio* calculation of surface states of sulfide minerals: pyrite, chalcopyrite and molybdenite

G. U. VON OERTZEN, S. L. HARMER and W. M. SKINNER*

ARC Special Research Centre for Particle and Material Interfaces, Ian Wark Research Institute, University of South Australia, Mawson Lakes, SA 5095, Australia

(Received October 2006; in final form October 2006)

Sulfide minerals contain sulphur in a large variety of coordination environments. Consequently, the S 2p XPS of various mineral surface states undergo different shifts in binding energy (BE) relative to the bulk, depending on the charge distribution on the surface. This in turn depends on the number, type and position of the atoms on the fracture surface, which is determined by the fracture mechanism.

We have investigated three sulfide minerals: pyrite (tetrahedrally-coordinated S), chalcopyrite (tetrahedrally-coordinated S) and molybdenite (layered structure with trigonally-coordinated S). Comparison of conventional with surface sensitive synchrotron XPS shows that the S 2p spectrum displays two additional doublets at lower BE than the bulk signal for pyrite, and one doublet each at lower and at higher BE for chalcopyrite. Each of these signals is derived from surface states. Molybdenite shows no additional states. A BE shift to lower (higher) BE suggests a charge increase (decrease) on the S atoms relative to those in the bulk because of higher (lower) charge screening.

We have used *ab initio* density functional calculations to validate this interpretation of the experimental evidence, obtaining Mulliken population analyses for the possible fracture surfaces and comparing their charge distribution with the corresponding bulk charge distribution. Our calculations support the assignments of S 2p surface contributions as follows: the lower BE peak of chalcopyrite (160.84 eV) as under-coordinated surface S states, the higher BE peak of chalcopyrite (161.88 eV) as surface S polymers, the lowest BE peak of pyrite (161.3 eV) as surface S monomers, and the next lowest BE peak of pyrite (162.0 eV) as under-coordinated surface S dimers. The absence of any surface states in molybdenite is also confirmed by the models.

Keywords: Sulfide minerals; *Ab initio* quantum chemical calculations; X-ray photoelectron spectroscopy; Surface states

1. Introduction

Chalcopyrite (**$CuFeS_2$**, space group $I\bar{4}2d$, figure 1) is an antiferromagnetic semiconductor with a structure similar to that of sphalerite. In chalcopyrite, four Zn atoms of sphalerite are replaced by two atoms of Fe and Cu each, with the S atoms remaining unchanged [1]. The Fe and Cu positions are alternated in the lattice; the unit cell size in the *z*-direction is doubled from the cubic sphalerite. The antiferromagnetic nature of chalcopyrite results from the alternation of high-spin Fe^{3+} with opposite polarity in successive layers in the *z*-direction. Chalcopyrite displays poor cleavage in any direction. Both sulphur and metal atoms are tetrahedrally-coordinated—each S atom to four metal atoms and each metal atom to four S atoms, respectively.

Pyrite (**FeS_2**, space group, $Pa\bar{3}$ figure 2**)** is a common iron sulfide mineral in nature and is a semiconductor. Industrially, pyrite has applications in solar energy conversion [2,3], Li/FeS_2 batteries [4,5] and, potentially, hydrogen generation [6,7]. Pyrite is cubic with Fe atoms at the corners and face centres of the cube, and S—S dimer pairs cantered on the cube edges and at the centre of the cube [1]. The orientation of the dumbbell-shaped S—S dimers is respectively parallel to the four different body diagonals. Sulphur atoms are tetrahedrally-coordinated to one S and three Fe atoms, while Fe atoms are octahedrally-coordinated to six S atoms. Pyrite displays poor cleavage in the {001} directions.

Two different geometries are generally given for **molybdenite** (**MoS_2**); hexagonal, space group $P6(3)/mmc$ (figure 3) or trigonal, space group: $R3m$ (figure 4). As molybdenite is a layered structure, the difference between the two is in the detail of the layer stacking. In the trigonal form, stacking forms three distinct layers, whereas

*Corresponding author. Email: bill.skinner@unisa.edu.au

Molecular Simulation
ISSN 0892-7022 print/ISSN 1029-0435 online © 2006 Taylor & Francis
http://www.tandf.co.uk/journals
DOI: 10.1080/08927020601081616

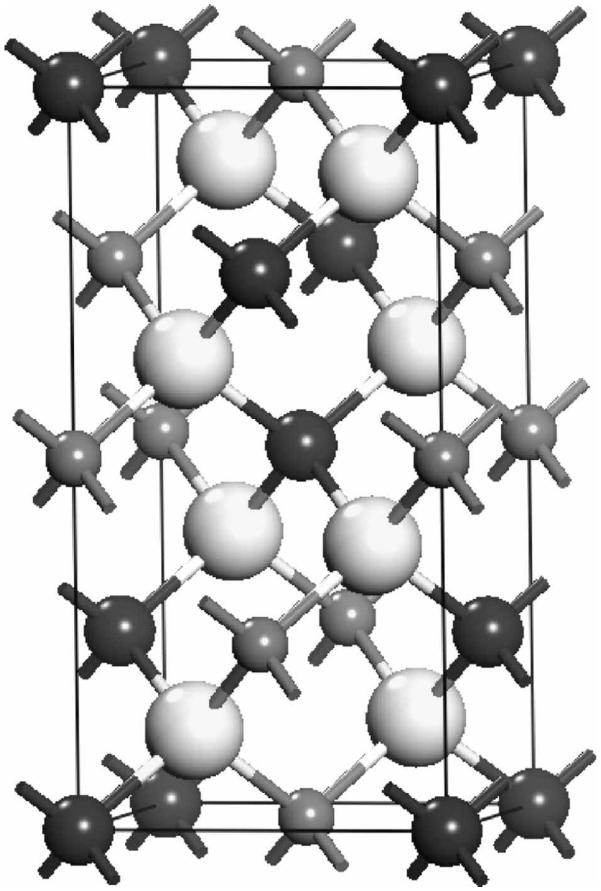

Figure 1. Conventional unit cell for chalcopyrite. In this an all the following ball and stick diagrams, large light grey spheres denote S atoms, small dark grey circles denote Cu atoms, and medium-sized medium grey spheres denote Fe atoms. The *z*-direction is down in this figure.

in the hexagonal form there are only two distinct layers. This makes no difference to the binding properties, however, as in both cases S atoms are trigonally-coordinated to Mo atoms, which in turn are six-fold coordinated to two planes of S atoms arranged in a triangle, one each above and below the Mo atom. The layer structure results in perfect (0001) cleavage.

2. Method

2.1 Experimental

Sulphur 2p core-line spectra of the vacuum fractured mineral surfaces were collected using a Kratos Axis Ultra X-ray photoelectron spectrometer with a monochromatic Al Kα source. The source spot size used was 300 × 700 μm. High resolution scans of the S 2p lines were collected at 10 eV pass energy. The spectrometer was calibrated using the metallic Cu $2p_{3/2}$ and Cu $3p_{3/2}$ lines. Surface contributions to the spectral intensity were minimized by collecting all spectra at a take-off angle normal to the sample surface. Pristine surfaces of samples

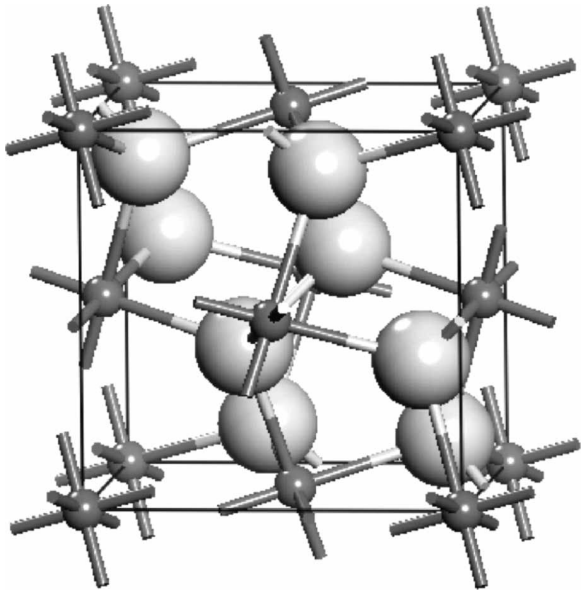

Figure 2. Conventional unit cell for pyrite.

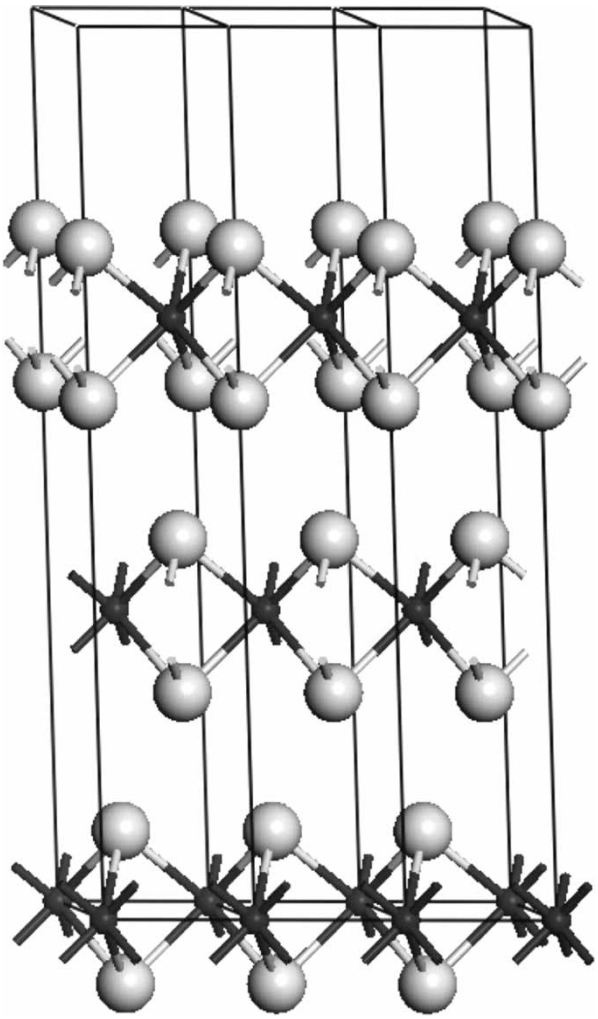

Figure 3. Row of 3 conventional unit cells for molybdenite R3m. In this and all following ball and stick diagrams, tiny dark spheres denote Mo atoms.

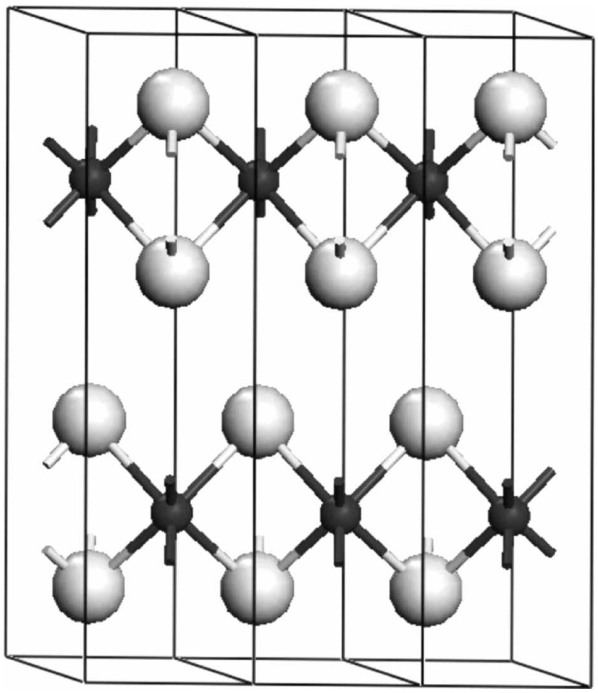

Figure 4. Row of 3 conventional unit cells for molybdenite P6(3)/*mmc*.

of pyrite and chalcopyrite were prepared by fracture in vacuum ($\sim 10^{-6}$ Pa) in the electron spectrometer preparation chamber before XPS analysis. Molybdenite surfaces were prepared by peeling to reveal a fresh surface just prior to pump down.

Synchrotron Radiation X-ray Photoelectron Spectroscopic (SR-XPS) experiments were performed using the HERMON beam line at the University of Wisconsin Synchrotron Radiation Centre. The line utilizes a spherical, variable line density grating and a special grating translation/rotation mechanism with which to minimize grating aberration effects such as defocus, coma and spherical aberrations over the entire scan range [8,9]. For slits of 10 mm, the energy resolution of the monochromator varies between $\Delta E = 50-100$ meV over the scan range of the low energy grating ($E = 50-550$ eV) and between $\Delta E = 50-200$ meV over the range 500–1100 eV [10]. Samples were cleaved *in situ* in the preparation chamber (about 10^{-7} Pa) and transferred in vacuum to the photoemission chamber with typical pressure of 10^{-8} Pa during data accumulation. The S 2p spectrum was taken at 50 meV photon energy resolution. The samples were cooled at liquid helium temperature during analysis using photon energies in the range 245–450 eV. The surfaces of the minerals were prepared in an identical fashion to those for conventional XPS.

2.2 Theoretical

The geometry optimization and population analysis calculations herein were performed using Materials Studio CASTEP [11], a density functional theory (DFT) based plane-wave pseudopotential program within which the generalized gradient approximation (GGA) has been employed [12], using the Perdew-Burke-Ernzerhof (PBE) exchange-correlation functional [13]. Ultrasoft pseudopotentials were used within a plane wave basis with cutoff energy of 300 eV.

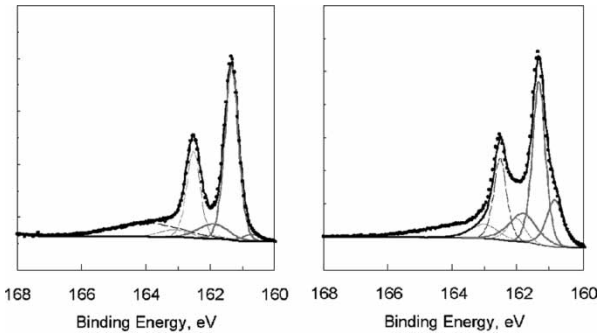

Figure 5. Conventional (left) and Synchrotron (250 eV excitation, right) XPS of the S 2*p* core line in chalcopyrite.

3. Results and discussion

3.1 Experimental

The conventional and synchrotron (250 eV excitation energy) XPS of the S 2p corelines of the three minerals is shown in figure 5 (chalcopyrite), figure 6 (pyrite) and figure 7 (molybdenite). The conventional S 2p XPS spectra of the three minerals are very similar to each other, displaying a strong doublet originating from the spin–orbit splitting into $p_{1/2}$ and $p_{3/2}$ peaks. In accordance with quantum theory, the ratio of the peak areas is 2:1 ($p_{3/2}$:$p_{1/2}$), with $p_{3/2}$ being at the lower BE, respectively. When comparing the spectra with the Synchrotron counterparts at 250 eV, the distinguishing features of the spectra become clear. At this low excitation energy, the emitted photoelectrons typically traverse between 1 and 4 monolayers before being attenuated, in contrast to about 20 monolayers in the case of conventional spectra at an excitation energy of 1487 eV. Consequently, about 40% of the SXPS signal should originate from the surface, whereas in the conventional case this contribution is reduced to a few percent.

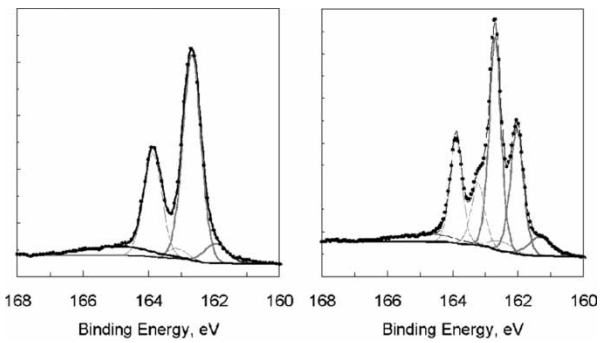

Figure 6. Conventional (left) and Synchrotron (250 eV excitation, right) XPS of the S 2*p* core line in pyrite FeS_2.

The chalcopyrite SXPS signal displays a low BE shoulder as well as a significant contribution to the signal between the bulk $p_{1/2}$ and $p_{3/2}$ peaks. As shown by Harmer *et al.* [14], a good fit is achieved with three spectral spin–orbit contributions: the bulk S signal at $2p_{3/2}$ BE of 161.33 eV, a lower-BE peak at 160.84 eV and a higher-BE peak at 161.88 eV. Harmer *et al.* [14] have ascribed the low-BE doublet to surface S monomers and the high-BE peak to surface S polymers.

The pyrite SXPS signal displays two low BE peaks. As shown by Nesbitt *et al.* [15], a good fit is achieved with three spectral spin–orbit contributions, the bulk S signal at 162.6 eV, and two lower-BE signals at 162.0 and 161.3 eV, respectively. The two lower-BE peaks have been ascribed by the same authors to surface S dimer (162.0 eV) and surface S monomer (161.3 eV) contributions.

The molybdenite XPS and SXPS (figure 7) are practically identical—a single doublet is therefore a sufficient fit for both.

3.2 Theoretical

The XPS spectra of pyrite and chalcopyrite suggest the presence of different S species on the surface, whereas this does not seem to be the case for molybdenite. On fracture, bonds between the ligand (S) and metal ions are broken. The ligands in compound semiconductors typically retain the bonding electrons; an increase in (negative) charge on ligand atoms, therefore, results on breakage of bonds. Increased charge leads to an increase in shielding, thus lowering the BE of the S 2*p* orbitals, amongst others. An increase (decrease) in BE therefore suggests a decrease (increase) in negative charge (electrons) on the respective surface S atom relative to the S atoms in the bulk.

Chalcopyrite displays poor cleavage, and any fracture will therefore be a combination of different surfaces. The two most likely surfaces for fracture are shown in figure 8. The (012) surface exposes the same number of metal and S atoms, and there is therefore only one unique surface. The (11 − 2) surface exposes only S atoms on one side and only metal atoms on the other side of the cut, resulting in two different surfaces. A (012) slab, when fully relaxed without any constraints to the central atoms of the slab, is extremely unstable and relaxes into an unsymmetrical

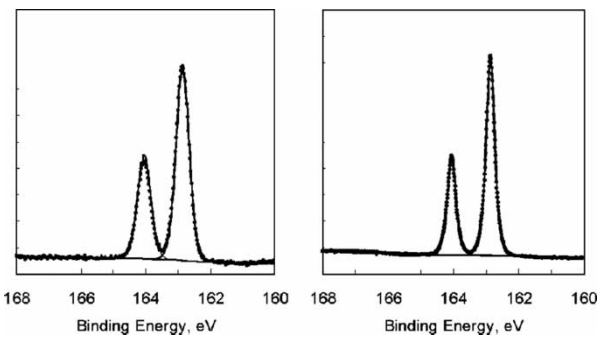

Figure 7. Conventional (left) and Synchrotron (250 eV excitation, right) XPS of the S 2*p* core line in molybdenite.

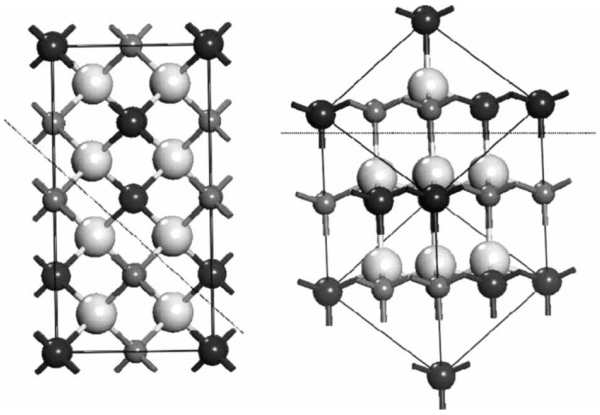

Figure 8. Left: Cut to arrive at the (012) surface. Right: Cuts to arrive at the (11 − 2) surface.

irregular structure. The relaxation of the (11 − 2) surface is even more dramatic when the central layers are not constrained. When constraining all but the top two surface layers, the (11 − 2) surface exposing metal atoms remains very unstable, with significant relaxation, while the one exposing S atoms is relatively stable. The surface relaxation of the surface exposing metal atoms is in such a way as to achieve a rearrangement exposing the lower-lying S atoms instead.

We show a (11 − 2) slab in figure 9, with an exposed surface of S atoms at the top of the slab and a surface of exposed metal atoms at the bottom of the slab. After geometry relaxation, the structure of the slab is changed to expose S atoms at both types of surface. In addition, the exposed S monomers on the top surface form polymer chains by binding to each other. The Mulliken charges of the exposed S monomers show that those S monomers which have formed S polymer chains have their negative charge decreased when compared to the fully coordinated S atoms in the bulk layer below (to a positive value in this case). This is in agreement with the interpretation by Harmer *et al.* [14] who have assigned the S 2*p* core BE shift to higher BE to the formation of S polymers.

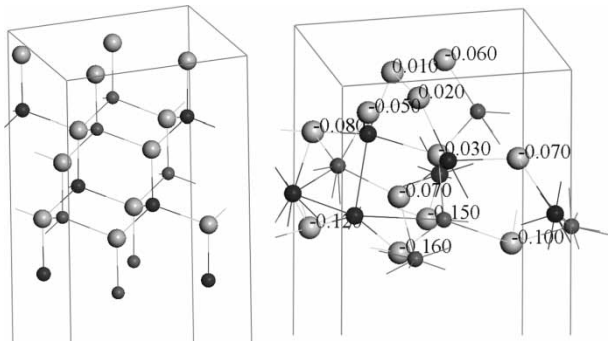

Figure 9. (11-2) slab of chalcopyrite, with S monomers exposed at the top and metal atoms exposed at the bottom. Left: before relaxation, and right, after relaxation, showing the Mulliken charges of S atoms. Note that the four S monomers at the top surface have formed bonds with each other.

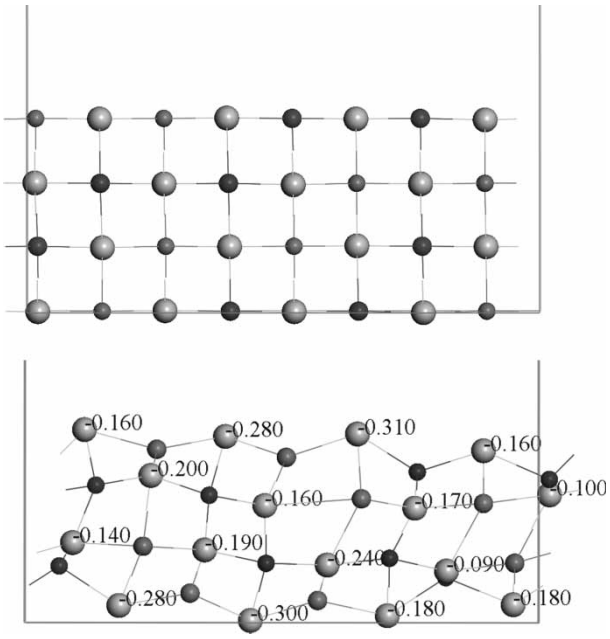

Figure 10. (012) slab of chalcopyrite, before (top) and after (bottom) geometry optimization. Mulliken charges are given for the S atoms of the relaxed structure.

A (012) slab is shown in figure 10. Again, the relaxation is in such a way as to expose the S atoms. The Mulliken charges of under-coordinated S atoms (those exposed on the surface, both at the top and the bottom of the slab) are clearly reduced over those of the fully coordinated S atoms in the bulk layers below. This is consistent with the interpretation of Harmer *et al.* [14] who have assigned the S 2*p* core BE shift to lower BE to under-coordinated S atoms on the surface.

Pyrite does not display perfect cleavage—therefore the (001) surface will contain proportions of Fe—S and S—S bond rupture as shown in figure 11. The top line results in a bulk terminated surface with Fe—S bonds between layers broken, but no S—S dimer bonds are broken. The bottom line results in a surface in which, in addition, S—S

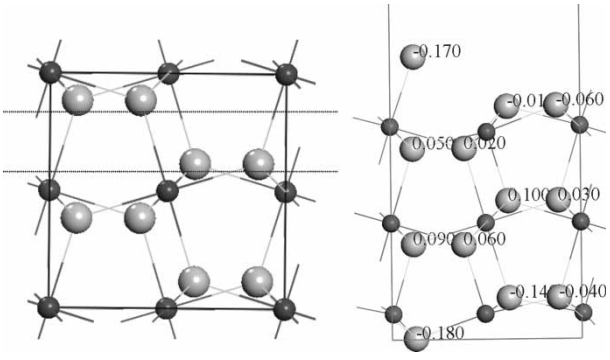

Figure 11. Left: Possible surface cuts of pyrite (001). Right: A combination (001) pyrite surface (right), containing both surface S monomers and S dimers. Mulliken charges are given for the S atoms, and the surface is at the top of the figure, with the structure below the surface representing several layers of bulk.

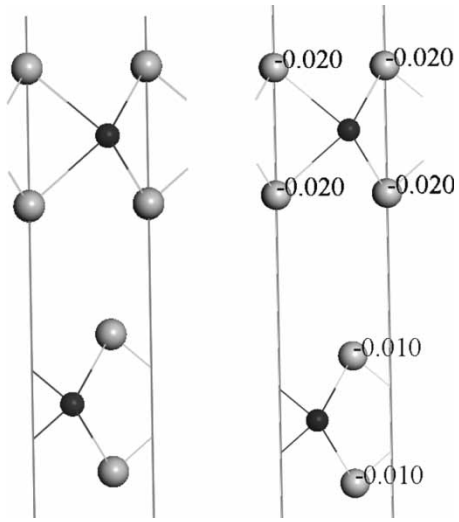

Figure 12. Left: Side-on view of molybdenite (R3 m) with red dotted line denoting cleavage direction. Right: molybdenite surface (at the top of the figure), with the structure below the surface denoting several layers of bulk. Mulliken charges are given for S atoms.

bonds are broken and which therefore contains surface S monomers. The real surface is a combination of these cases. A geometry optimisation of the bulk terminated (001) surface shows this to be absolutely stable, with no appreciable surface relaxation. When retaining surface monomers on the (001) surface, this is still very stable, with only a small lateral relaxation of the surface monomers and no relaxation of the layers below them. A Mulliken population analysis (while not giving correct absolute values, nevertheless a good tool to demonstrate relative trends) shows the charge distribution on a modelled surface. The surface monomer clearly has the largest negative charge, followed by the slightly smaller charge on the topmost surface S dimers. The bulk dimers have an even smaller charge (positive in this case). This is consistent with the interpretation of Nesbitt *et al.* [15] of assigning the lowest BE peak to S monomers and the next-lowest BE peak to S surface dimers, as shown by von Oertzen *et al.* [16].

Molybdenite has perfect cleavage in the direction separating layers, so only one type of surface in this crystal direction is possible (figure 12). The Mulliken population analysis shows that the bulk and surface S charges are almost identical, explaining the absence of any potential surface state peaks in the XPS spectra. This is immediately understandable, as the bonding between layers is not covalent, but of the van der Waals type. Bonds are therefore not broken on cleavage, and the surface S atoms have the same coordination as those in the bulk.

4. Conclusions

The S 2*p* spectra, taken with conventional (1487 eV excitation) and synchrotron (250 eV excitation) XPS, respectively, were compared for chalcopyrite, pyrite and

molybdenite. *Ab initio* quantum chemical calculations were performed for the minerals in question, by performing a geometry optimisation of crystal slabs. A Mulliken population analysis of the relaxed structures was then used consistently to confirm the interpretation of the core line shift features observed:

- In chalcopyrite, two additional peaks are observed, a lower BE peak ascribed to under-coordinated surface S atoms and a higher BE peak ascribed to the formation of S polymer features.
- In pyrite, two additional lower BE peaks are observed, ascribed to the presence of both surface S monomers (lowest BE) and under-coordinated S dimers (lower BE than bulk, but higher than monomer contribution).
- In molybdenite, only one S $2p_{3/2}$ peak is observed, consistent with the fact that no S bonds are ruptured during cleavage and therefore the S atoms on the surface are not under-coordinated as they are in most other sulfide minerals.

Acknowledgements

This work was supported by the Australian Research Council through the Special Research Centre for Particle and Materials Interfaces and The Australian Mineral Science Research Institute (AMSRI). We acknowledge the use of CPU time under the Australian Partnership for Advanced Computing (APAC)'s Merit Allocation Scheme. We also wish to acknowledge funding for the Synchrotron Radiation Centre (Univ. of Wisconsin) via NSF award no. DMR-95-31099 and travel assistance through the Australian Synchrotron Research Program, which is funded by the Commonwealth of Australia under the Major National Research Facilities Program.

References

[1] W.A. Deer, R.A. Howie, J. Zussman. *An Introduction to The Rock-Forming Minerals*, 2nd ed., Longman, London (1992).

[2] P. Altermatt, T.F. Kiesewetter, K. Ellmer, H. Tributsch. Specifying targets of future research in photovoltaic devices containing pyrite (FeS2) by numerical modeling. *Solar Energy Mater. Solar Cells*, **71**(2), 181 (2002).

[3] S. Nakamura, A. Yamamoto. Electrodeposition of pyrite (FeS2) thin films for photovoltaic cells, solar energy materials and solar cells. *Solar Energy Mater. Solar Cells*, **65**(1–4), 79 (2001).

[4] J.-W. Choi, J.-K. Kim, Y.-H. Kim, J.-U. Kim, J.-H. Ahn. Electrochemical properties of primary Li/FeS_2 batteries. *Mater. Sci. Forum*, **486-487**, 658 (2005).

[5] S.-H. Yang, S. Osmialowski, Q.C. Horn. Nano-FeS_2 for commercial Li/FeS_2 primary batteries. *J. Electrochem. Soc.*, **149**(11), 1499 (2002).

[6] S.B. Lalvani, M. Sharmi. Pyrite-assisted water electrolysis. *Int. J. Hydrogen Energy*, **10**(7-8), 447 (1985).

[7] Z. Yongfeng, L. Hongjie, C. Haiyong, Y. Ying, Z. Yajie. Simultaneous production of hydrogen and oxidation of pyrite slurries. *Int. J. Hydrogen Energy*, **17**(10), 763 (1992).

[8] H. Höchst, M. Bissen, M.A. Engelhardt, D. Crossley. Design study of a high resolution soft X-ray monochromator with a movable variable groove density grating. *Nuclear Inst. Meth. Phys. Res. A*, **319**, 121 (1992).

[9] M.V. Fisher, N. Steinhauser, D. Eisert, B. Mason, F. Middleton, H. Höchst. Combining rotation and translation in a variable line space high-resolution soft-X-ray monochromator: Design requirements and performance evaluation of a novel grating mount. *Nuclear Inst. Meth. Phys. Res. A*, **347**, 264 (1994).

[10] M. Bissen, M. Fisher, G. Rogers, D. Eisert, K. Kleman, T. Nelson, B. Mason, F. Middleton. First results of SRC's new high-energy resolution variable line density grating monochromator beamline: HERMON. *Rev. Sci. Inst.*, **66**, 2072 (1995).

[11] M. Segall, D.P.L.D. Lindan, M.J. Probert, C.J. Pickard, P.J. Hasnip, S.J. Clark, M.C. Payne. First-principles simulation: ideas, illustrations and the CASTEP code. *J. Phys.: Cond. Matt.*, **14**(11), 2717 (2002).

[12] A.D. Becke. Density-functional exchange-energy approximation with correct asymptotic behavior. *Phys. Rev. A*, **38**, 3098 (1988).

[13] J.P. Perdew, K. Burke, M. Ernzerhof. Generalised gradient approximation made simple. *Phys. Rev. Lett.*, **77**, 3865 (1996).

[14] S.L. Harmer, A.R. Pratt, H.W. Nesbitt, M.E. Fleet. Sulfur species at chalcopyrite ($CuFeS_2$) fracture surfaces. *Am. Miner.*, **89**, 1026 (2004).

[15] H.W. Nesbitt, G.M. Bancroft, A.R. Pratt, M.J. Scaini. Sulfur and iron surface states on fractured pyrite surfaces. *Am. Miner.*, **83**, 1067. Sulfur and iron surface states on fractured pyrite surfaces. American Mineralogist, 83, 1067 (1998).

[16] G.U. von Oertzen, W.M. Skinner, H.W. Nesbitt. *Ab inito* and x-ray photoelectron spectroscopy study of the bulk and surface electronic structure of pyrite (100) with implications for reactivity. *Phys. Rev. B*, **72**, 235427 (2005).